Bulletin of Engineering Geology and the Environment (2026) 85:309
https://doi.org/10.1007/s10064-026-04984-2

ORIGINAL PAPER

Recognizing bedrock deformation zones through integrated 3D modelling of bedrock topography and sedimentary deposits, Turku, SW Finland

Kati M. Ahlqvist[1] · Pietari Skyttä[2] · Noora Anttila[3] · Antti E.K. Ojala[1,3] · Eemi Ruuska[3]

Received: 23 September 2025 / Accepted: 3 April 2026

Abstract

Urban development along the Baltic Sea coast requires high-resolution subsurface information to support effective planning and construction. This study presents a 3D geological model of the subsurface in the City of Turku, SW Finland, based on selected geotechnical investigations, Quaternary superficial deposit maps and LiDAR data. The model comprises three components essential for engineering geological assessments: a digital elevation model of the bedrock surface, the distribution and thickness of coarse grained glacial sediments, and the overlying fine-grained clay deposits.

A major part of the analysis focuses on the bedrock surface, which shows a complex and heterogeneous topography shaped by several sets of deformation zones. These structures form linear valley-like depressions that strongly influence the geometry of sedimentary basins and the thickness patterns of both coarse- and fine-grained deposits. The integrated model reveals previously undescribed deformation-zone geometries, including a continuous NE–SW-trending system and subsidiary structures, providing new insights into the brittle architecture of the Turku bedrock.

The result show how bedrock-controlled depressions have guided sediment accumulation and produced characteristic basin-fills relevant for engineering evaluations. In addition to characterizing the deformation zone framework, the 3D model provides region-wide outputs, including bedrock elevation variations, sediment thickness patterns and the spatial distribution of superficial deposits. These results demonstrate that existing geotechnical investigations, when carefully selected, can effectively support high-resolution subsurface modelling in dense urban environments. When data coverage is limited, additional geotechnical investigations and geophysical surveys are recommended to improve model reliability.

Keywords 3D geological modelling · Bedrock surface · Deformation zone · Quaternary deposits · Fennoscandian shield · Finland

Introduction

Land use in urban areas requires understanding of diverse geological constraints, including the properties of unconsolidated sedimentary deposits and the underlying bedrock, and their contribution to the engineering conditions. With specific reference to cities along the Baltic Sea coast, land use and underground development has shifted into areas with less favourable ground conditions and thicker deposits of fine-grained unconsolidated sediments, which places challenges upon planning and construction. The need to understand and anticipate the behaviour of the ground under loading conditions has become increasingly important in these areas (Fookes 1997; Ojala et al. 2021; Saresma et al. 2021). Within this context, detailed thickness maps and 3D models of bedrock surface and the overlying sediments provide a practical framework in making realistic assumptions about the properties and the 3D arrangement of the involved geological materials (Fookes 1997; e.g. Culshaw 2005; Devleeschouwer and Pouriel 2009; El May et al.

✉ Kati M. Ahlqvist
kati.ahlqvist@gtk.fi

[1] Geological Survey of Finland, P. O. Box 96, Espoo 02151, Finland

[2] Structural Geology Company Oy, Kaniikintie 3, Turku 20300, Finland

[3] Department of Geography and Geology, University of Turku, Turku 20012, Finland

Published online: 14 April 2026

2010; Collon et al. 2015; Wang et al. 2018). Moreover, 3D geological models and associated information on geological materials deliver value to land use and infrastructure projects through risk assessment and reduction, planning and efficiency savings, and timely decision-making processes.

Regional-scale 3D geological modelling essentially comprises surface and subsurface datasets such as digital elevation models (DEM), seismic reflection profiling, and geological maps of bedrock and Quaternary deposits (e.g. Artimo et al. 2003; Heinonen et al. 2012), whereas data useful for more detailed locale-scale subsurface modelling are more limited in terms of spatial density, spatial coverage and consistency. For the latter case, geotechnical investigations (including drillings and penetration tests) form the primary source of subsurface data; however, despite the high density of investigation points, their spatial coverage is often uneven and discontinuous, and limited to specific areas. In urban areas geotechnical investigations are typically spatially clustered at the sites of large construction or along infrastructure routes such as railway or highway corridors, or a site of large construction. Moreover, the bulk of data often comprises input from different types of investigations and data storage methods acquired during extended time periods (up to several decades), and consequently, the data contains errors in the quality and in the variable documentation. For the reasons above, geotechnical investigation datasets often remain scattered and unorganized, and only a share of the available data is directly usable for compiling comprehensive subsurface geological 3D models that extend beyond specific target areas.

The present study showcases a 3D modelling approach comprising a systematic review and filtering of originally heterogeneous geotechnical datasets, their merging with light detection and ranging (LiDAR)-derived DEMs and compilation of integrated high-resolution geological 3D models. Part of this work builds upon a project conducted for the City of Turku, during which two MSc theses were completed (Ahlqvist 2023; Anttila 2023). The project produced 3D models of the bedrock surface and overlying sediments for urban planning purposes and to improve understanding of local subsurface conditions. These earlier models provided input for the data integration workflow and the conceptual framework applied here.

The resulting 3D models provide seamless representations of the bedrock surface and the overlying glacial and postglacial sediments in the City of Turku, SW coast of Finland. Specifically, the present study characterizes (i) the topography of the partially exposed surface of the glacially eroded crystalline bedrock, (ii) the areas of occurrence and thickness variation of coarse-grained cohesionless glacial sediments (diamicton, gravel, sand) occurring predominantly within the topographic lows upon bedrock surface, and (iii) the overlying fine-grained and cohesive clayey sediments forming extensive fills within depositional basins of diverse sizes and shapes. The bedrock surface and the stratigraphic contacts between the sedimentary units define a conceptual geological 3D model of the ground (comprising bedrock and sediments), which allow realistic construction of integrated 3D models of the data.

As a primary component of the subsurface, bedrock forms the depositional basement for the overlying sediments and controls on the deposition processes and thicknesses of glacial and postglacial sediments. The primary control over the bedrock surface morphology within formerly glaciated terrains occurring in areas of crystalline bedrock is attributed to selective glacial erosion, where the intensely fractured deformation zones have experienced enhanced erosion and appear as elongate topographic depressions (Krabbendam and Bradwell 2014; Skyttä et al. 2015). This relationship between deformation zones and their associated structural elements, such as joints, extension fractures, shear fractures and fault-related damage zone fracturing, is particularly evident in areas with exposed bedrock (Skyttä et al. 2023). In contrast, the detailed morphology of the bedrock surface within depressions characterized by thick sedimentary deposits is much more uncertain, because in such areas the presence and geometry of the underlying deformation zones must be inferred indirectly e.g. from geophysical data (Skyttä et al. 2015; Malinowski et al. 2023; Ruuska et al. 2023). Within the present study area, the highly variable bedrock surface morphology is attributed to two sets of deformation zones: one that is linear and continuous and typically oriented NE-SW, and another that is shorter and more irregular in character, and represents intersections or branches of this dominant orientation (Niemelä et al. 1987). The large-scale geometry and continuity of these deformation zones have not been described in detail. However, Väisänen and Hölttä (1999) have described that these zones are associated with directly observed deformation structures such as subvertical shear zones with mylonitic foliation and pseudotachylyte, S–C fabrics and asymmetric porphyroclasts, demonstrating localized strain. Furthermore, according to previous work by Niemelä et al. (1987) the thickest successions of coarse-grained sediments, with up to 40 m thickness, occur within these fracture-controlled bedrock depressions, which also host the thickest deposits of clay (up to 50 m). However, the extent and thickness variation of diverse sedimentary deposits, and the shapes of the clayey basins are thus far largely unknown.

In southern Finland, according to Björck (1995) and Ojala (2011) the ground behaviour and engineering-geological properties of the subaqueously deposited Baltic Sea Basin (BSB) sediments depend on the composition of clays and sedimentary environment in which they were initially

deposited (Gardemeister 1973; Ojala et al. 2018). Ojala et al. (2018) used an allostratigraphic approach to spatially constrain two main types of the late- and postglacial fine-grained sediment units with different characteristics and engineering-geological properties along the southern coast of Finland. These lithologies are separated by an erosional unconformity in a form of a sand layer (Virtasalo et al. 2014). The underlying part is composed of glaciolacustrine varved clay/silt-sand and postglacial weakly layered lacustrine silty clay. The overlying part is composed of brackish water organic-rich muds that are often softer (greater plasticity index and liquid limits), bioturbated, and contain naturally elevated concentrations of sulphide bearing minerals (Fe-monosulphide) (Ojala et al. 2018). The significance of the two-fold division from land use and construction perspective relates to the higher abundance of sulphide minerals, low strength and unfavourable consolidation properties of the upper unit, potentially resulting in the development of acid sulphate soils and ground instability (Edén et al. 2023; Ojala et al. 2021).

This study documents the first comprehensive 3D models of bedrock surface topography and the overlying glacial and postglacial deposits (clayey basins) in and around the City of Turku. Construction and analysis of the 3D models aimed at (i) developing new understanding about which approaches and work-flows should be implemented for optimal use of geotechnical investigation datasets in 3D geological modelling, (ii) providing new insight into the deformation zones within the bedrock, including their geometry, topology and surface morphology through selective glacial erosion, (iii) evaluating how bedrock surface topography controlled the successive basin infills during the progressive phases of the BSB development, and the resulting total sedimentary thickness, and (iv) characterizing different types of sedimentary environments and basin geometries during the BSB phases using Benthic Terrain Modeler (BTM). We expect that the approaches and experiences from the present study will provide guidance for 3D geological modelling in other regions of similar geology.

Geological setting

The present study area in Turku, SW coastal area of Finland displays a combination of Precambrian bedrock and Quaternary glacial and postglacial deposits, with bedrock outcrops covering 35% and fine-grained (clay) deposits 40% of the terrestrial land surface (Fig. 1). The geological settings are essentially similar to those along the southern coast of Finland described by Ojala et al. (2021) and Saresma et al. (2021). The present study area is located within the Southern Svecofennian domain of Finland, which is characterized by high-grade metamorphism and polyphase structural evolution during the prolonged Svecofennian orogenesis at 1.9–1.8 Ga (Ga = billion years ago; giga-annum) (Väisänen and Hölttä 1999; Lahtinen et al. 2005; Skyttä and Mänttäri 2008). According to Väisänen and Hölttä (1999) the crustal evolution comprises an early thrust-related stage with development of the main rock fabric and synchronous emplacement of sheeted tonalite intrusions into the supracrustal successions at 1.89–1.87 Ga. Another main episode followed at 1.84–1.83 Ga, comprising refolding of earlier fabrics, generation of doubly plunging folds with sheared ENE-WSW trending limbs, intense migmatization and emplacement of granite dykes along fold axial surfaces. As a result, the bedrock structures and the lithological units define an overall NE-SW to ENE-WSW trend, shaped by intense late-orogenic deformation and associated ductile shear zones located at fold limbs. This structural trend is locally cut by subvertical N-S to NNE-SSW trending late-orogenic semi-brittle shear zones that Väisänen and Hölttä (1999) attributed to a stage of regional uplift.

The study area was beneath the Fennoscandian Ice Sheet (FIS) during the last glacial maximum (LGM) at around 20–22 ka (ka = thousand years; kilo-annum) ago, and prior to that it has been covered by a continental ice sheet several times during the Late Pleistocene (e.g. Donner 1995; Palacios et al. 2022). At the time of LGM the FIS covered all of Fennoscandia and northern Germany in the south and had advanced over the present study area from the NNW (340–350°) direction (Palacios et al. 2022). During the late Weichselian deglaciation the FIS had retreated to Salpausselkä zone in southern Finland at around 12 700 cal BP (cal BP = calibrated years before present, where "present" = AD 1950) and by that time was organized into lobate ice flow sectors and sub-sectors (Boulton et al. 2001; Stroeven et al. 2016). Ice sheet re-advance in lobate flow form during the Younger Dryas forming the Salpausselkä ice-marginal complexes (Donner 1995). The study area is in the Baltic Sea Ice Lobe sector, which is characterised by the three major Salpausselkä ice-marginal formations (I, II and III Salpausselkäs). The present study area lies about 40 km up-ice from the III Salpausselkä ice-margin position. Deglaciation of the study occurred around 10 700 cal BP during the Yoldia Sea phase in the Baltic Sea basin history (Stroeven et al. 2016). At the time of deglaciation, a proglacial sea level was 130 m above the present-day sea level (m a.s.l.) in the Turku area (Glückert 1976; Ojala et al. 2013). The highest hills (60–80 m a.s.l.) in Turku were isolated from the BSB during the Ancylus Lake to Litorina Sea transition at around 8000–9000 cal BP, but most parts of Turku were still under the BSB at 4000 cal BP (Fig. 2). The isolation of the present study area from the BSB has mostly occurred during the

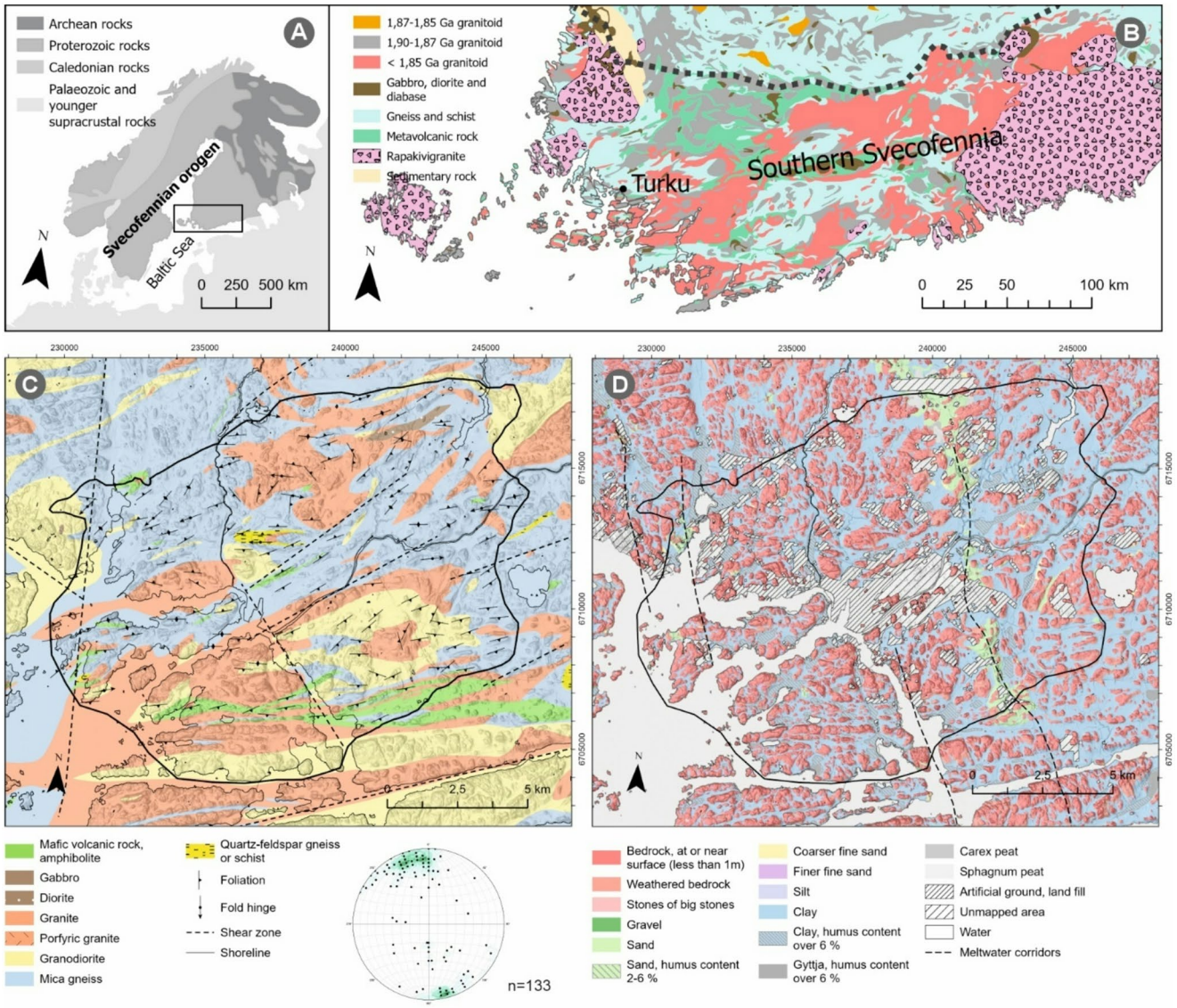

Fig. 1 (**A**) Geological overview of the Fennoscandian Shield and (**B**) Lithological map of Southern Svecofennia, modified after Koistinen et al. (2001). The dashed line marks the northern boundary of the Southern Svecofennian domain. (**C**) Bedrock lithology, shear zones, foliation (stereoplot) and structural observations of the study area, modified after Lindberg et al. (1994), Väisänen and Hölttä (1999) and Väisänen (2007). (**D**) Superficial deposits of the study area (Superficial deposits 1:20000, 2015 @ Geological Survey of Finland; hereafter GTK) and meltwater corridors modified after Niemelä et al. (1987). The present study area in the City of Turku is given with black solid line. Multidirectional hillshading was generated using digital elevation model (Elevation model 2 m, 2024 @ National Land Survey of Finland; hereafter NLS)

last two millennia, with the present isostatic glacial uplift of 5 mm per year.

Stratigraphic studies by Hirvas and Nenonen (1987) and Bouchard et al. (1990), among others, indicate that glacial erosion across southern Finland was significant during each glacial phase and the majority of pre-Late Weichselian glacial sediments were transported towards the south (Patton et al. 2022). Only scattered remains of pre-Late Weichselian deposits are known in southern Finland (e.g. Hirvas et al. 1995) so the landscape is nowadays dominated by bedrock outcrops and landforms and sediments deposited during the Late Weichselian and postglacial BSB phases (Fig. 1D). Due to the glacial history, till layers in the study area are generally thin (0.5–2 m), however, Niemelä et al. (1987) report that some bedrock deformation zones may contain up to 20–40 m thick deposits of coarse-grained till and sand sediments. There are four, roughly north to south oriented meltwater corridors in the area that follow the N-S oriented bedrock deformation zones (Fig. 1C). Some sections of these corridors are characterized by broken glaciofluvial esker deposits (Glückert 1976; Niemelä et al. 1987), especially the one that pass through the eastern sector of

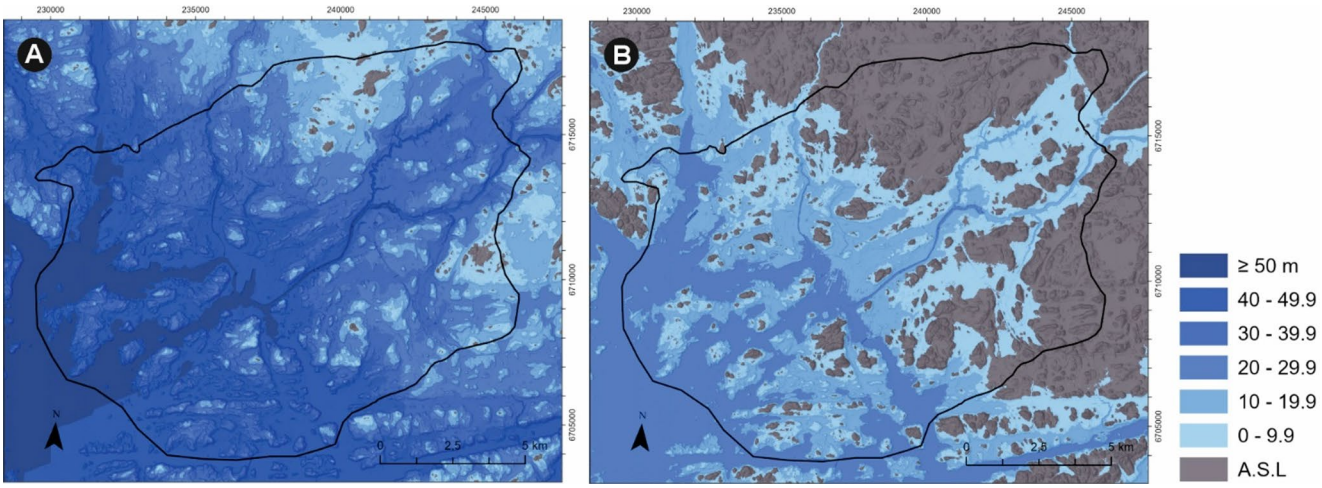

Fig. 2 Water depth in the Turku area (**A**) 8000 cal BP and (**B**) 4000 cal BP, modified after Ojala et al. (2013). Multidirectional hillshading as background image, was generated using digital elevation model (Elevation model 2 m, 2024 @ NLS)

the City of Turku. Late Weichselian glacial deposits (till, gravel, sand) are mostly overlain by up to 50 m thick deposits of fine-grained postglacial sediments (silt and clay) of the BSB, which, combined with bedrock outcrops, are the dominant geological features of the present study area.

Datasets and methods

The datasets used in the present study contain Quaternary maps of superficial deposits (1:20 000), LiDAR digital elevation models (2 and 10 m grids) with processed derivatives such as multidirectional hillshading (MDHS), aerial photographs and Google Street View imagery, and geotechnical investigations (Table 1). In total, about 60 000 datapoints of geotechnical investigations were present in the study area such including data from Swedish weight soundings, vane tests, cone penetration tests with pore water pressure measurements (CPTU), and different types of percussion drillings to the bedrock. Of these, about 50 000 include a soil type interpretation, while the remaining investigations consist solely of penetration test data.

The 3D geological model of the Turku area was constructed using the available above-mentioned data and following the procedures of previous studies, including data integration, interpretation, interpolation and finally 3D modelling (e.g. Culshaw 2005; Ojala et al. 2021). For consistency and applicability for civil engineering purposes, we designed our geological conceptual model of the subsurface 3D elements as straightforward as possible, and in a manner that unit sub-division is relevant from the perspective of material properties and geotechnical behavior (Knill 2003). Our conceptual 3D elements contain the following units:

Table 1 Datasets used in 3D geological modelling the bedrock surface and the thickness, upper and lower surface of the clay deposits

Dataset	Description / data format	Source
Geotechnical investigation data	INFRA	City of Turku and GTK
Ground surface LiDAR DEM, 2 m resolution	Grid size 2 × 2 m Geo Tiff	NLS
Ground surface LiDAR DEM, 10 m resolution	Grid size 10 × 10 m Geo Tiff	NLS
Superficial deposits at 1 m depth	1:20 000 Soil type at 1 m depth; modified RT-classification; Esri geodatabase	GTK
Clay points	Pirilä (2016) clay observation points XYZ point data; csv	Pirilä (2016)
Satellite, aerial and outcrop images	Google Maps and Google Street View -imagery	Google
Bedrock Map	Bedrock of Finland; 1:200 000	GTK
Field observations	Site visits in 12/2021	

- Geological Unit 1 (Unit 1): The partially exposed and partially covered erosion surface of the crystalline bedrock. Bedrock surface acted as the depositional basement for the overlying sedimentary deposits and hence defines the basal layer for 3D-modelling. Modelling of Unit 1 aims at generating a digital elevation model of the bedrock surface (hence called 'bedrock-DEM'), which adequately represents the previously recognized small-scale topographic variations (Niemelä et al. 1987) and, consequently, provides understanding about the lateral variation in depth to bedrock for modelling the sedimentary deposits.
- Geological Unit 2 (Unit 2): Cohesionless coarse grained glacial sediments that directly overlie the bedrock and

comprises of two sub-units; unsorted tills and glacifluvial sorted sands and gravels, which were deposited during the glacial progress and retreat, respectively. Separation of the above sub-units is neither meaningful due to their largely similar engineering properties, nor possible to conduct reliably using the available geotechnical datasets, and, consequently, the unit remains undivided in our models. The bottom boundary of Unit 2 is a sharp unconformity to underlying Precambrian bedrock, but associated with an uncertainty, which relates to the investigation method and the reliability of the interpreted type of termination of the geotechnical drilling data (Sect. 3.1).

- Geological Unit 3 (Unit 3): Cohesive clayey basin fill deposits representing a diverse syn- and postglacial phases of the BSB and overlying postglacial mud and peat layers, which were deposited after the isolation. The bottom boundary of Unit 3 may not always be unequivocally defined due to both the gradational transition from glacifluvial sand to postglacial silt and clayey deposits, and post-depositional shoreline processes, that cause erosion and redeposition of littoral sands into the basins (see e.g. Ojala et al. 2021). An intent to distinguish and determine a boundary between Units 2 and 3 is conducted as it is essential due to their highly contrasting geotechnical behavior.

For simplicity, Unit 2 was essentially modelled as a solid above the bedrock surface and below postglacial clayey deposits. The main reasons for this were that in the study area there are no exposures of till and gravel/sand sediments within the glacial sequences so the determination of cohesionless material is solely based on geotechnical data which means it is very uncertain.

3D modelling of bedrock surface

We compiled the bedrock-DEM (Unit 1) mostly through integration of geotechnical data and LiDAR DEM for unexposed sediment covered and exposed areas of bedrock, respectively (See Table 1 for full listing of the data used). For the exposed parts of the bedrock, we used the following workflow: (i) Delineation of the outcrop margins using hillshaded 2 m grid LiDAR DEM, distribution of the known occurrences of clay ('clay points'; Pirilä 2016), supported by Google Street View and field observations (Fig. 3). (ii) Resampling of the resulting bedrock outcrop margins to 10 m node density and vertical projection of the nodes on the 10 m ground surface DEM. (iii) Extraction of elevation points (LiDAR DEM 10 m) within the bedrock outcrop areas, inside the outcrop margins and merging with the points representing the outcrop margins (point ii). The total number of the delineated bedrock outcrop exposures in the study area was 1 387 (Fig. 3D), and these comprise a total of 468 095 surface-based (LiDAR DEM 10 m) elevation points.

For the unexposed parts of the bedrock, we used the following workflow: (iv) Filtering of geotechnical data into two subsets (Fig. 4): (a) investigations which were confirmed to terminate in the bedrock ('confirmed') and (b) investigations which terminated by wedging, or against a rock or a boulder, or bedrock, but the type of termination had not been confirmed by drilling a minimum 3 m into the bedrock ('unconfirmed'). For the unconfirmed points we added 2 m of depth so that it would better represent the bedrock surface elevation at that point ('interpreted bedrock points'). This choice is supported by an analysis of percussion drillings where both the coarse grained deposit immediately above the bedrock surface and a verified bedrock contact were recorded. For these cases ($n=2$ 848), the thickness of the overlying coarse grained deposits had: mean 2.37 m, median 1.50 m, 25th percentile 0.80 m, 75th percentile 2.80 m, range 0.10–35.10 m. A uniform 2 m correction is therefore (i) less than the mean, (ii) between the median and the 75th percentile, and (iii) consistent with the typical thickness of the coarse grained layer over the bedrock surface in the study area. Consequently, termination against "rock/boulder/wedging" is expected to occur close to the bedrock surface rather than far above it. This is consistent with observations that subglacial traction and lodgement processes produce coarse, boulder-rich material immediately at or near the bedrock surface, frequently with large clasts embedded in till at the ice–bed interface (Boulton 1978). This approach was corresponding to that conducted by Lindqvist et al. (2025) when modelling bedrock surface of Otaniemi region in southern Finland.

Prior to bedrock surface modelling, the geotechnical data were subjected to visual quality control. Fewer than ten observations (<0.05% of the dataset) were excluded due to clearly erroneous bedrock depth records that were inconsistent with surrounding observations and interpreted as data entry or recording errors. In cases where conflicting bedrock elevations were recorded at the same location, the lower elevation value was retained for modelling because upper bedrock interpretations are more prone to error (e.g. refusal on boulders or dense sediments).

The spatial distribution of the geotechnical data was clustered, with dense coverage in central parts of the study area and lower sampling density toward the margins. Local comparison of neighboring observations indicated generally good internal consistency, while a small proportion (approximately 2%) of points showed locally conflicting values. These were interpreted as reflecting natural geological variability rather than systematic measurement errors.

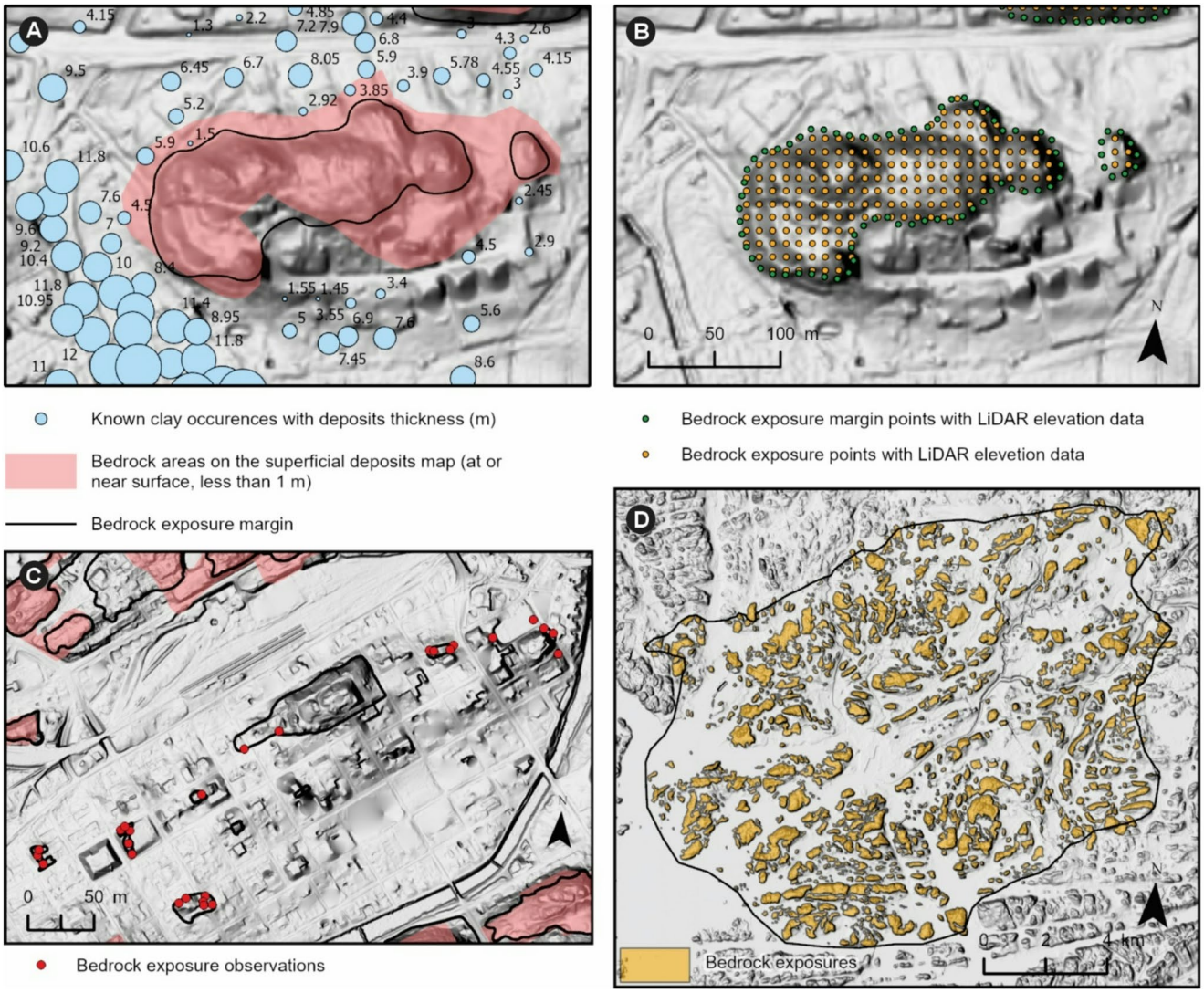

Fig. 3 The approach used in extracting the elevation point dataset for the exposed parts of the bedrock. (**A**) Improved delineation the extent of bedrock exposures. Note that the outcrop areas in Superficial deposits maps by the Geological Survey of Finland comprise areas with less than 1 m of overburden whereas the digitized outline polygon of the outcrop in this study corresponds to zero overburden. (**B**) Extracted LiDAR elevation points for the areas of outcropping bedrock. (**C**) Complementary bedrock exposures resulting from field observations acquired in this investigation. (**D**) An overview of all the bedrock exposures with no overburden. Multidirectional hillshading as background image, was generated using digital elevation model (Elevation model 2 m, 2024 @ NLS)

Model performance was evaluated using cross-validation within the Empirical Bayesian Kriging framework in ESRI® ArcGIS Pro. The mean prediction error was close to zero, indicating negligible systematic bias. The root-mean-square error was approximately 1 m, corresponding to less than 1% of the total elevation range of the modeled bedrock surface. Larger residuals were spatially limited and occurred mainly in areas of sparse data coverage or abrupt geological transitions. Overall, the close agreement between predicted and observed values supports the reliability of the modeled bedrock surface within the resolution of the available data.

The total number of confirmed bedrock points was 5 982 and there were 27 427 interpreted bedrock points in the present study area. We then exported the geotechnical data into a XYZ point cloud using 3D-Win software package (Novatron Oy) and converted the data into an MS Excel CSV file, which is suited for surface interpolations. Finally, (v) we merged the datasets covering the exposed and unexposed parts of the bedrock into a unified point cloud and used it to interpolate the bedrock-DEM with ESRI® ArcGIS Pro (Geostatistical Analyst/Empirical Bayesian Kriging), using 30 m grid size. As a final step, we clipped the resulted bedrock-DEM to match the outline of the study area, excluding offshore areas, as no depth-to-bedrock data was portrayed for those regions (Fig. 4A, B).

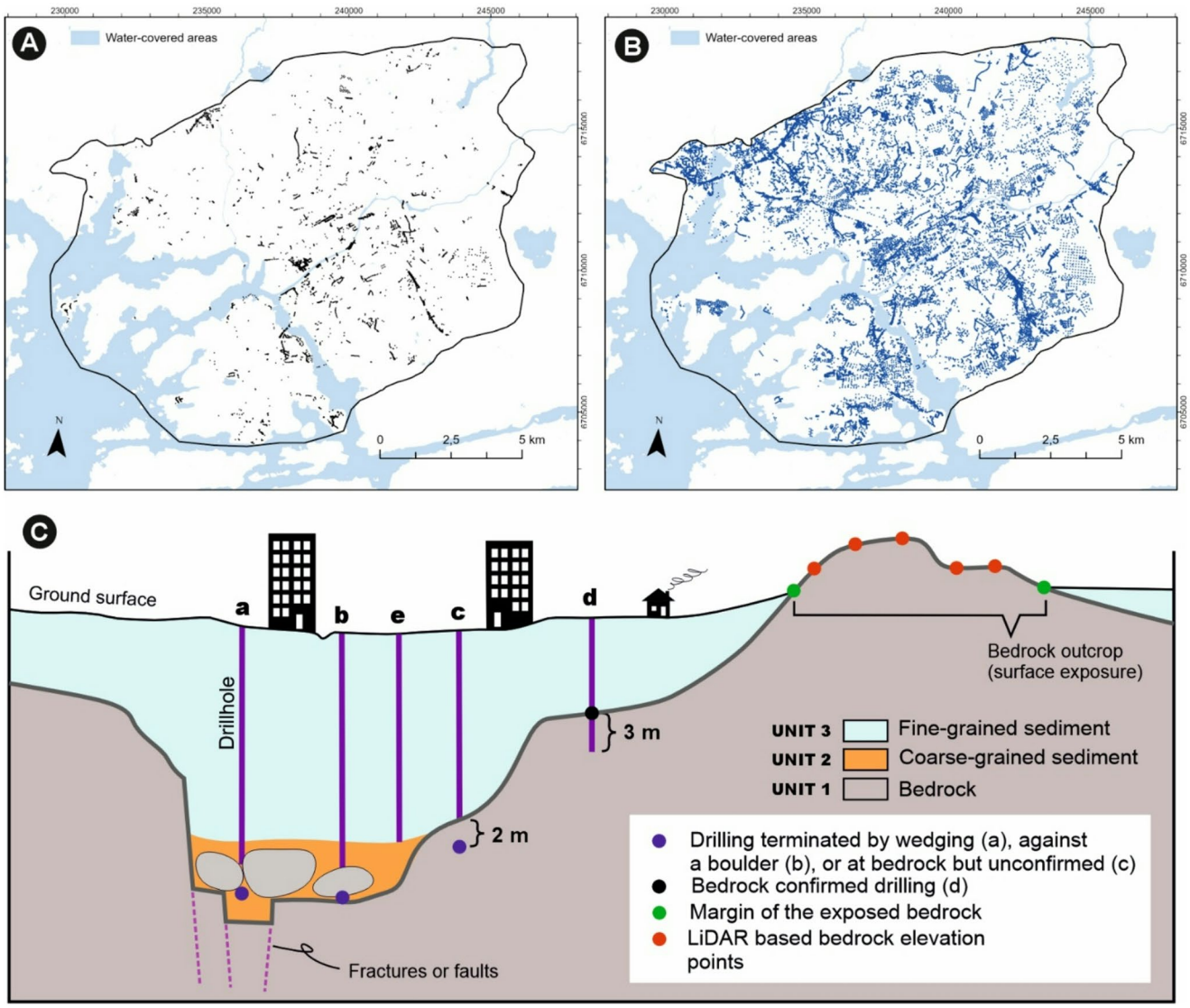

Fig. 4 The dataset and approach used in extracting the elevation point dataset for the unexposed parts of the bedrock. (**A**) 'Confirmed' bedrock points where drilling was confirmed to terminate at bedrock. (**B**) 'Unconfirmed' bedrock points where termination of the drilling at or close to the bedrock is inferred but not confirmed. The present-day shoreline and river network, modified after Finnish Environmental Institute 2021; is used in applying the blue mask for the water-covered areas. (**C**) A conceptual cross-section illustrating the modelled geological units and different types of associated input data

3D modelling of clay thickness

The datasets used for clayey thickness and surfaces modelling (Unit 3) were compiled through integration of point data from geotechnical investigations, LiDAR DEMs and existing maps of Quaternary superficial deposits (See Table 1 for full listing of the used data).

Delineation of Unit 3 was based predominantly on three types of geotechnical investigation methods: Swedish weight sounding tests (SWS), field vane tests and cone penetration tests with pore water pressure measurement (CPTU). First, (i) for clayey areas we selected investigation points that documented fine-grained deposits (clay) in sediment strata (29 804 points out of 57 694) (Fig. 5A). These points were used for determination of clay thickness and lower boundary of clayey section based on previous interpretation by Pirilä (2016), operator remarks, and by calculations of the strength parameter from results of SWS tests. For interpretation of a lower boundary of clayey sequence, we used a value where SWS resistance exceeds 20 half-turns, which is in an agreement with that of Pirilä (2016) and an operator note on sediment types where available (Fig. 5B). Similar approach has previously been adopted by Ojala et al. (2021) and Saresma et al. (2021, 2023). Where multiple elevations were available at the same location, the mean value was used in order to represent the average interpreted depth of

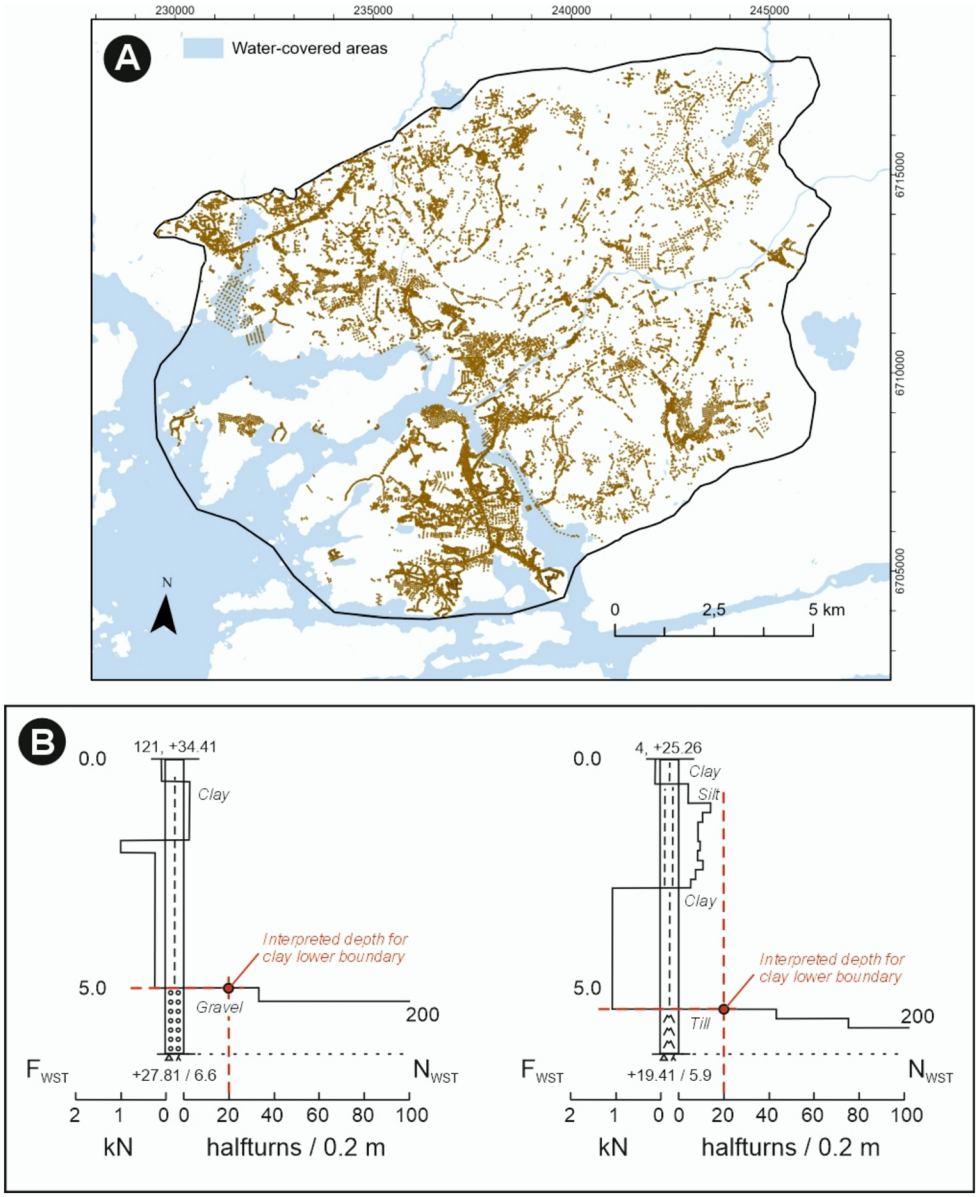

Fig. 5 (**A**) Geotechnical investigation points of fine-grained deposits (clay) in sediment strata ($n = 29\,804$), (**B**) Examples of geotechnical investigation diagrams illustrating the interpretation of the lower boundary of clay based on SWS resistance exceeding 20 half-turns

the interface. This approach is appropriate for sedimentary contacts, which are typically gradational rather than sharply defined, and therefore subject to small interpreter-specific variations. Using the mean reduces the influence of local anomalies and produces a more stable and geologically representative surface for interpolation.

The spatial distribution of the data was clustered, with higher investigation density in intensively studied areas and lower density elsewhere. Average Nearest Neighbor analysis confirmed a strongly clustered sampling configuration (Nearest Neighbor Ratio = 0.41, $p < 0.001$), indicating spatially variable data density across the study area. Model performance was assessed using cross-validation within the Empirical Bayesian Kriging framework in ESRI® ArcGIS Pro. The mean prediction error was close to zero, indicating negligible systematic bias. The root-mean-square error (2.89 m) represents approximately 2.5% of the total elevation range of the lower boundary of clay (−51 m to +65 m), indicating good relative predictive performance at the scale of the study area. Larger residuals were spatially limited and occurred primarily in areas of sparse sampling or where the clay–substrate boundary changed abruptly over short distances, reflecting small-scale basal topography or sedimentary heterogeneity. Taken together, the data density, internal consistency of the observations, and agreement between modelled and observed values support the reliability of the lower boundary of clay surface model within the spatial resolution of the available dataset.

For the exposed and non-clayey areas, we used the following workflow: (ii) Delineation of the clay margins (‘zero

level' of clay) using hillshaded 2 m LiDAR DEM, topographic maps, aerial photographs, distribution of the known occurrences of clay in ground surveys (as above), and 1: 20 000 Quaternary maps. (iii) Resampling the 'zero level' of clay along the outlines at 2 m node density. (iv) Extraction of elevation points for clay margins (m a.s.l.) from topographic models with the same 10 m node resolution applied for bedrock exposures (Unit 1). During this process, we carefully reviewed that bedrock outcrops exposures were outside and all geotechnical investigation points indicating clay was inside the area of fine-grained sediments.

Finally, (v) in accordance with bedrock surface modelling, we integrated the surface- and subsurface point datasets into a common point cloud and interpolated the clay thickness and lower boundary with ESRI® ArcGIS Pro (Geostatistical Analyst/Empirical Bayesian Kriging), using 30 m grid size. In the last step, we clipped the resulted models with the outline of the study area, the marine area within the coastal zone, and with areas above the level zero of clay deposits.

In order to classify paleotopography of the study area proglacial basin soon after deglaciation and before the onset of clay deposition, we used Benthic Terrain Modeler (BTM) (Walbridge et al. 2018) that is built on top of the ESRI® ArcGIS platform. The tool computes slope, bathymetric position index (BPI) and rugosity from the input surface, and develops a reproducible and objective classification of depressions, slopes and crests (Lundblad et al. 2006; Kaskela et al. 2012; Rinne et al. 2014; Walbridge et al. 2018). We applied this tool to the lower boundary of clay in order to investigate the types of sedimentary basins and clay deposition dependence on the underlying bedrock topography following an approach previously applied in southern Finland (Saresma et al. 2021). Using the same catalogue, cell size (10 m), and parameter settings ensures regional comparability with earlier studies and avoids subjectivity inherent in manual interpretation.

3D modelling of coarse-grained sediment deposits

In our modelling approach, Unit 2 is considered as a (solid) 'layer' of coarse-grained deposits that occurs above the bedrock surface (Unit 1) and below the clayey deposits (Unit 3) (Fig. 4C) and is composed of cohesion sediments (till, gravel and sand) resistant to freezing and thawing. Modelling of Unit 2 did not involve delineation of any specific surfaces as the bottom and top surfaces for this unit correspond to the previously modelled top of Unit 1 and base of Unit 3 surfaces, respectively. Consequently, the vertical separation between the top and bottom surfaces indicates the thickness of Unit 2 and its spatial variability (using a 30 m grid size). Having deposited in a geologically recently glaciated terrain, Unit 2 comprises relatively thin till sequences from Late Weichselian glaciation that are overlain by glacifluvial gravel and sand deposited during deglaciation (Rainio and Lahermo 1976; Hirvas and Nenonen 1987). However, no further subdivision of Unit 2 into till/gravel/sand deposits were conducted due to the difficulty and subjectivity in recognition and interpretation of these layers from geotechnical data alone, which would eventually lead to unreliable results.

Results

Bedrock topography

Elevation of the interpolated bedrock-DEM (Unit 1) in the present study area ranges from 67.5 m above to 69.0 m below the present-day sea level (Fig. 6). Larger areas of higher bedrock elevation are dominant within the eastern sector, while more limited areas of bedrock highs occur throughout the entire study area. Areas of the lowest bedrock surface characteristically define elongate and relatively narrow valleys (e.g. Ia, b and IIa in Fig. 6) or wider domains bounded by linear structural discontinuities of the bedrock (IIb in Fig. 6). Moreover, depressions of irregular and non-linear shapes are present at the intersections of the narrow linear valleys, such as those appearing at the intersection between zones Ib and IIa (Fig. 6). Some of the linear depressions of the bedrock appear to be continuous into the marine areas, although the resolution is obscured by the lack of input data points from these areas.

Based on the orientation, the linear valleys of the bedrock can be subdivided into three groups with ENE-WSW, NE-SW and NNW-SSE trending directions (Fig. 6). The most continuous elongate depression is the ENE-WSW-trending feature (Ia) which occurs to the north of the Aurajoki river in the downtown area of Turku. The parallel depression underlying the Aurajoki river (Ib) shows the highest individual contrast in bedrock elevation from the −69 m level below the river to the +50 m high elevation bedrock exposures occurring just to the south of the river. These major depressions are adjoined by a few sub-parallel but less continuous zones to the south and north, that define a distinct ENE-WSW structural anisotropy in the bedrock surface topography in the central part of the study area.

Another distinct trend is defined by a swarm of NE-SW-trending depressions that are arranged in a spaced pattern within the eastern part of the study area (Fig. 6). The most pronounced of the NE-trending features is the Jaaninoja depression (IIa), which shows a maximum bedrock elevation contrast exceeding 100 m, is formed by successive 3–4 km long individual segments and can be traced for more

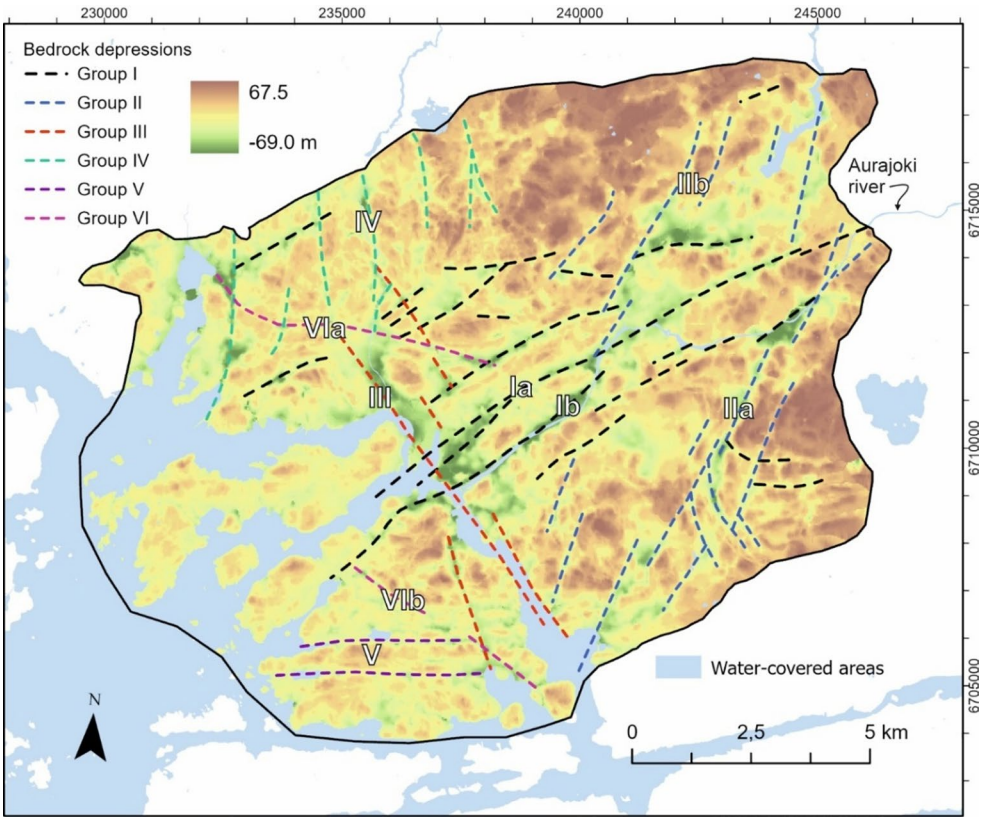

Fig. 6 Interpolated bedrock surface DEM (Bayesian kriging) overlain with distinct linear topographic depressions and structural discontinuities as recognized from the topographic patterns above and below the present-day sea level

than 12 km across the study area. The NE-SW-trending signatures and an area of relatively low bedrock surface elevations extend approximately 3.5 km west of the Jaaninoja depression, all the way until a similarly segmented NE-SW-trending structural zone (IIb). The NE-SW-trending zones (IIa, b) abut the more continuous ENE-WSW-trending zones.

The NNW-SSE-trending bedrock depression (III), which apparently separates the Turku mainland from the Turku archipelago, is defined by very low bedrock elevations in the north, but its depth-extent in the south could not be determined due to the lack of data in the marine areas (Fig. 6). However, the narrow straits between the mainland and the archipelago suggest that the zone has some continuity towards the south, whereas in the north the zone either deflects towards North (zone IV) or abuts a WNW-ESE-trending zone (VIa). Zone III is associated with a few parallel but shorter features within the closest 1.5 km in the east, and a sub-parallel branch in the south-west. The cross-cutting relationships between the ENE-WSW and the NNE-SSW -trending zones are not clear, but they appear to mutually crosscut each other.

The northwestern part of the study area is characterized by short (<3 km) N-S trending bedrock depressions (IV) that are less distinct than the earlier described ones. The N-S features are dominantly isolated and show no interaction with the other zones. The south-western study area displays a pattern of elongate, linear and parallel depressions (V) that are distinct, but where the associated contrasts between the lowest and highest bedrock elevation, similar to the N-S trending zones (IV), limited to some 50–70 m. Two further individual elongate depressions with WNW-ESE trends (VIa, b) were recognized in the western part of the study area. These features are not pronounced in elevation contrast, but have a moderate lateral continuity exceeding 5 km. The northern of the above features (VIa) abuts the ENE-WSW-trending major zones, while the cross-cutting relationship of the southern one (VIb) is less clear.

The calculated slope gradients for the bedrock surface DEM exceed a maximum of 50° in places, while the most common gradients range between 0–12° (Fig. 7). The steepest gradients are spatially associated with the main elongate depressions, with two zones standing out clearly due to their width, and particularly the lateral continuity of the steep gradients. These are the ENE-WSW trending depression underlying the Aurajoki River (Ia in Figs. 6 and 7A) and the NNE-SSW trending Jaaninoja depression (IIa in Figs. 6 and 7A). Both these zones are characterized by steep margins and flatter basal parts and exhibit an asymmetric character with steeper SSE slopes (Fig. 7). In the depression of the Aurajoki River, the southern slope is longer and steeper, and the narrow flat area in the bottom of the depression is clearly distinct (I in Fig. 7B). In the northeast (II in Fig. 7B),

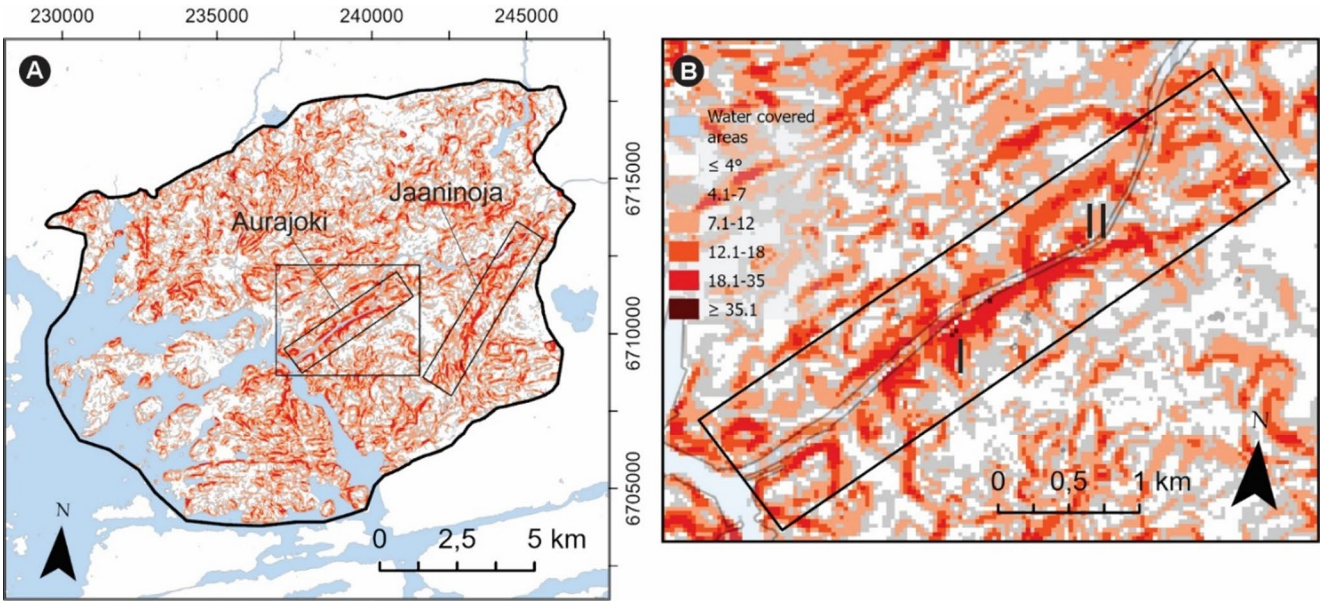

Fig. 7 (**A**) Slope gradients of the bedrock surface DEM, (**B**) The slope gradients of the Aurajoki depression

the valley-like structure disappears and is replaced by more small-scale topographic variation.

In cross-section, located at section I in Fig. 7, the Aurajoki bedrock depression has an asymmetrical shape with steeper SE slopes of approximately 33°, while on the NW side, the slope reaches a maximum of 18° (Fig. 8). In the cross-section, the bedrock surface is deeper towards the SE, verified by geotechnical investigations which are all located at the bottom of the depression (I in Fig. 8A). The investigations indicating the upper surface of the coarse-grained soil follow the topography of the bedrock surface, approximately two meters above the confirmed drillings. Due to the resolution, the small-scale variations indicated by the confirmed drillings are not visible in the interpolated bedrock surface (I in Fig. 8A). There are areas on both the NW and SE slopes where only unconfirmed drillings are present, and their inclusion in the modelling improves its reliability (II in Fig. 8A). In areas where there are neither confirmed nor unconfirmed drillings indicating the bedrock surface, parts of the interpolated surface seem to locate in too high elevation, because the upper surface of the coarse-grained soil layer is at the same level as the bedrock-DEM surface or even below it at the top of the southeast slope (III in Fig. 8). The representation of these poorly constrained areas could be further improved using 3D geological modelling software, which allows more robust extrapolation where data coverage is sparse.

Clay thickness and basins topography

Fine-grained sediments cover 58% of the study area (Fig. 9A). Because of the varying bedrock topography, the majority (51%) of sediment deposits are <3 m thick and >15 m thick deposits represent 10.5% of the total fine-grained sediment area. The thickest clayey deposits (Unit 3) clearly follow bedrock surface characteristics and are primarily located in elongated SW–NE-oriented bedrock valleys (Ia-Id in Fig. 9A), in a NW–SE-oriented valley (II in Fig. 9A), and in some basin-like areas in the north and northeast (III in Fig. 9A). These basin-like areas are wider in the NE (IIIa in Fig. 9A) than in the N (IIIb in Fig. 9A), where they form smaller, distinct, and evenly spaced deposits. The depth distribution of clayey deposits in the Turku area reflects the small-scale variation of the deposits and how the deepest layers effectively fill the largest bedrock depressions.

In the paleotopographic model, the lower surface of the fine-grained sediment ranges from −51 m to 65 m relative to the current sea level (Fig. 9B). The lowest elevations are found in areas with the thickest deposits, while in the NE and SE, where the bedrock surface elevation rises, the lower surface reaches up to 65 m. Near the seashore, the lower surfaces of thin clay deposits (<3 m) can also be relatively low, following the typical topographic trend of the area, where elevation increases with distance from the shore. Further inland, the lower surfaces of these thin clay layers are situated at higher elevations.

The basin topography has an essential role in the deposition of clayey sections and the coastal areas of Finland (e.g. Ojala et al. 2021; Saresma et al. 2021). Here, the paleotopographic model created using the Benthic Terrain Modeler (BTM), topographical variation is more distinct and abundant, with depositional environments that include elongated basins surrounded by wider depressions, which are

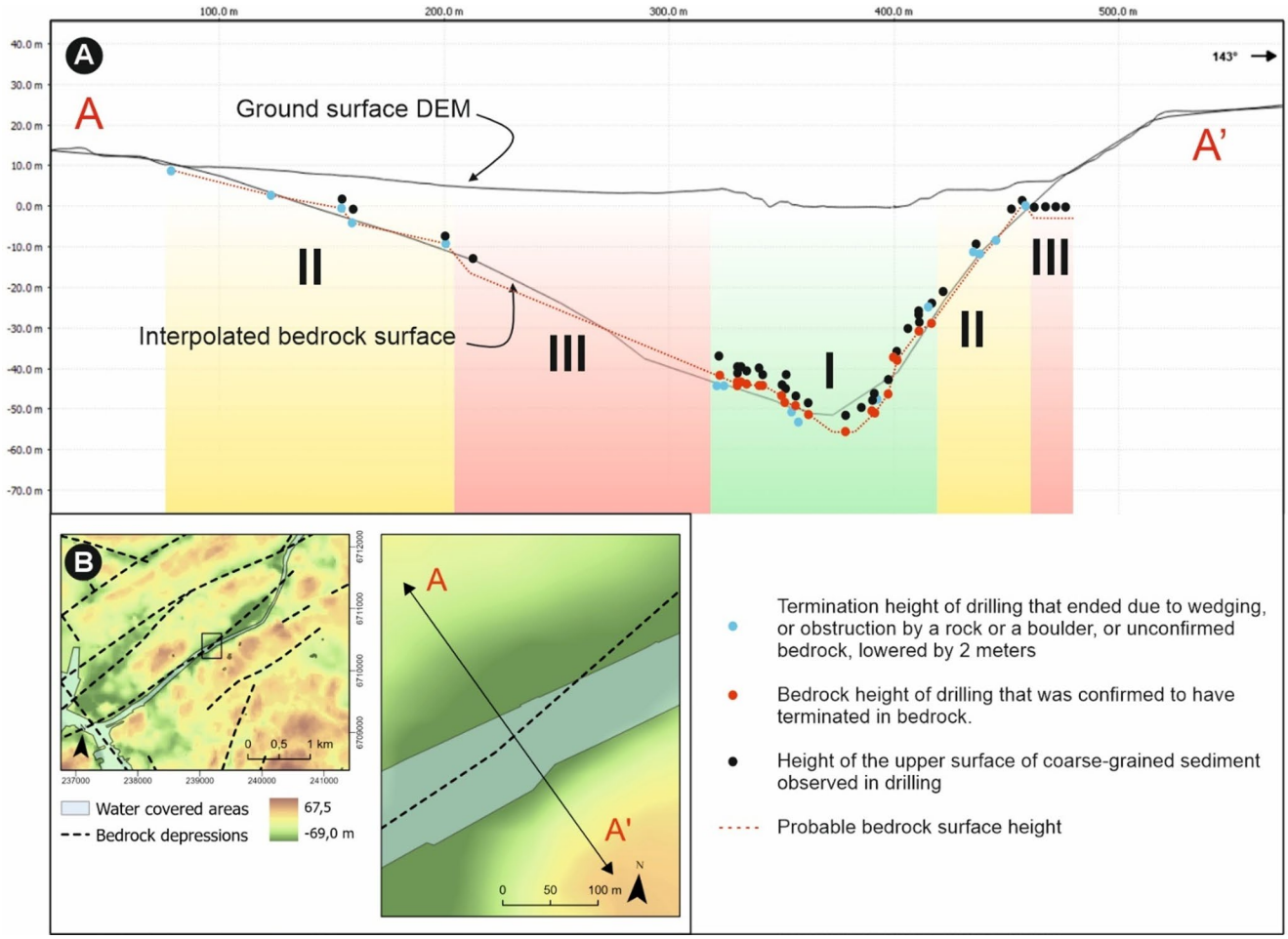

Fig. 8 (**A**) SE-NW cross-section of the interpolated bedrock surface and ground surface DEM at the Aurajoki River. Labels I–III refer to the availability of geotechnical data along the section. All zones contain investigations indicating the upper surface of the coarse-grained sediments. Zone I includes both confirmed and unconfirmed bedrock investigations, Zone II includes only unconfirmed bedrock investigations, and Zone III lacks both types of bedrock-surface-indicating investigations, making the bedrock surface interpolation more uncertain. (**B**) Location of the cross-section within the deformation zone of the Aurajoki River

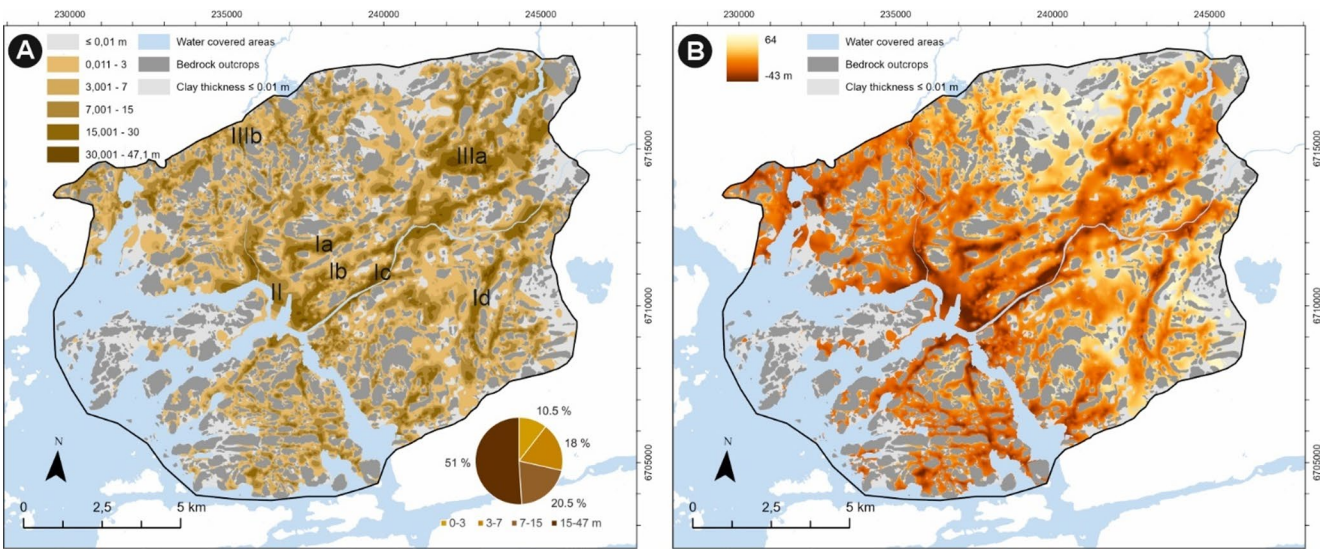

Fig. 9 (**A**) Clay thickness (Unit 3) and its percentage distribution in the study area, (**B**) The bottom level of the clayey fine-grained sediments

separated by isolating ridges and elevations (Fig. 10). These wider depressions form three larger basin-shaped areas: an elongated, NNW–SSE-oriented depression (I in Fig. 10) and two depressions in the northeast (II in Fig. 10), which connect to form a larger environmental complex through a continuous SW–NE basin (III in Fig. 10). Jaaninoja forms its own distinct depositional environment in SE (VI in Fig. 10), with a basin surrounded by a wide depression, eminences, and ridges. Outside the aforementioned areas, in the north, northwest, west, and southwest parts of the region, the depositional environments show smaller scale variation and are characterized not by extensive basins, but by small basins and depressions between ridges and small eminences.

Glacial coarse-grained sediments

The thickness of the coarse-grained glacial deposits (Unit 2) varies between 0 and 20 m (Fig. 11). The thickest deposits between the bottom surface of the fine-grained sediments and the bedrock surface are in areas where the bedrock surface reaches its lowest points, forming depressions. In the eastern part of the area lies the N-S-oriented Laitilanharju esker (Lounais-Suomen Seutukaavaliitto 1966; Niemelä et al. 1987; I in Fig. 11), where coarse-grained sediment deposits exceed 20 m in thickness. However, the esker's thickness is not continuous and it has a fragmented structure due to anthropogenic sand and gravel excavation activities (Lounais-Suomen Seutukaavaliitto 1966). Anomalously thick deposits are also found in the Aurajoki and Jaaninoja bedrock depressions, as well as on the east side of Raisionlahti (II in Fig. 11). In this area, deposits below the fine-grained deposits exceed 30 m in thickness. In the Aurajoki and Jaaninoja depressions, the thickness of the deposits varies. In the deepest areas, where the bedrock surface drops below −40 m a.s.l., the deposits are thickest, while they are thinnest on the slopes. In some slope areas, there is either no coarse-grained deposits at all or only a very thin layer, with fine-grained deposits resting directly on the bedrock surface.

Discussion

Deformation zones in the bedrock of the study area have controlled selective glacial erosion, resulting in topographic contrasts where certain narrow zones appear as depressions while other areas are variably elevated in character. This indicates a clear link between brittle deformation structures and present-day bedrock topography. Deformation zones form narrow, valley-like depressions, where the floors can be tens of meters deeper than the surrounding bedrock, often characterized by steep, flat basal part and asymmetrical slopes, indicating non-vertical dip. At intersections or terminations of deformation zones, broader basin-like

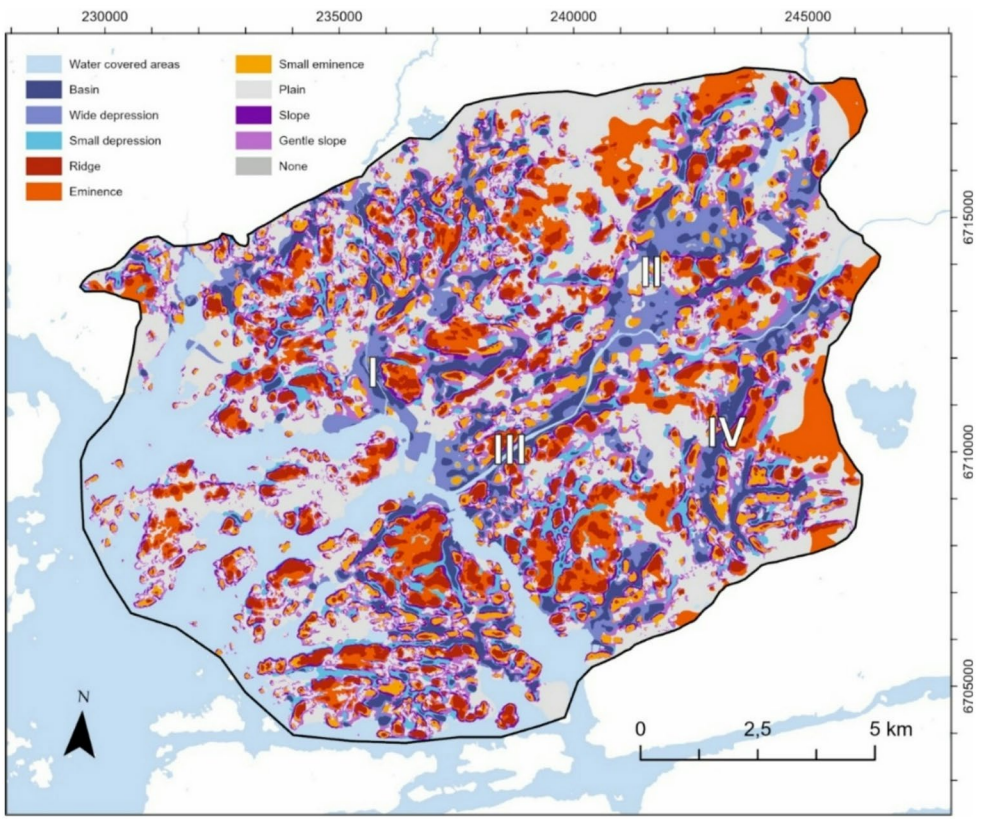

Fig. 10 Paleotopographic model of basin types prior to deposition of Baltic Sea basin sediments (clay = Unit 3) in the Turku study area created using the Benthic Terrain Modeler (BTM)

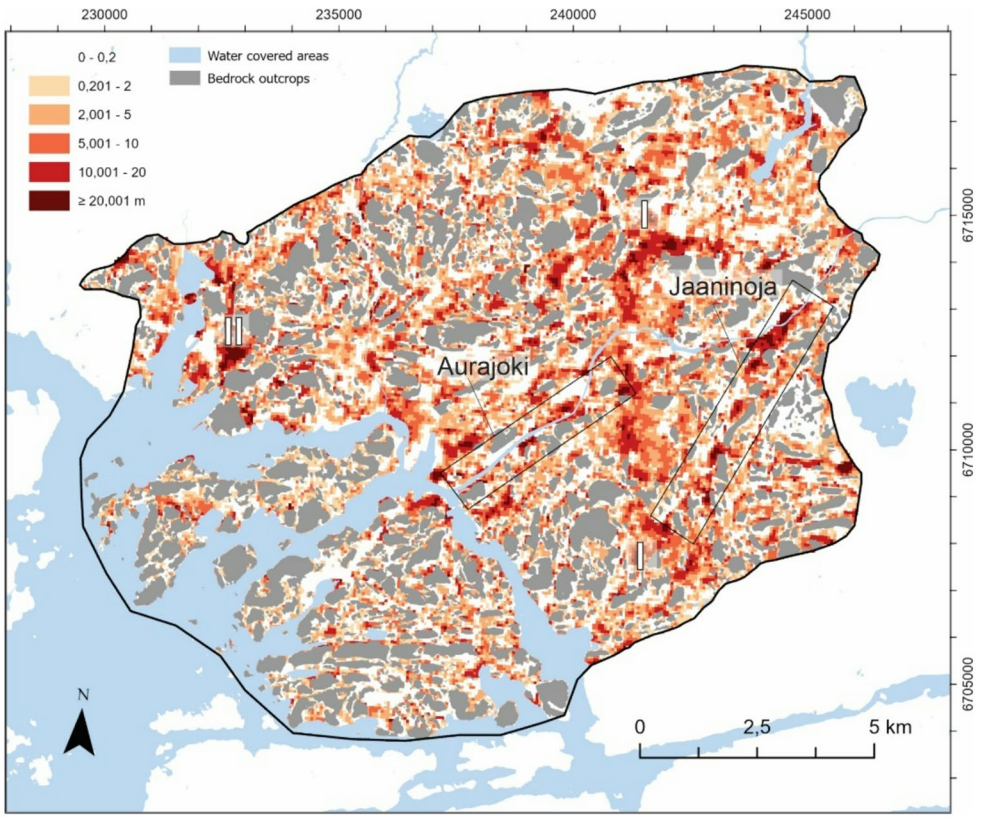

Fig. 11 The thickness of the coarse-grained deposit (Unit 2) in the Turku study area, calculated as the difference between the modeled clayey deposit (Unit 3) bottom level and the bedrock surface (Unit 1)

depressions with flat floors are present. The distinct asymmetry of the Aurajoki depression with steeper southern slope most likely reflects the architecture of the underlying bedrock deformation zone, and understanding their mutual relationships requires characterization of the outcrop-scale (1-10-100 m) brittle structures within the bedrock, which is out of the scope of this investigation.

The bedrock surface model produced in this study provides new insights into understanding the bedrock structures of localized deformation in the Turku region, as entirely new structures have been identified. Compared to the earlier interpretations (Lindberg et al. 1994; Väisänen and Hölttä 1999; Väisänen 2007), a third, longer ENE-trending deformation zone (Ia in Fig. 12A) has been identified, along with shorter, parallel zones to the north and south that continue offshore. Group II represents a completely new structural orientation unrecognized in the earlier work, defined by the continuous NE-trending Jaaninoja deformation zone (IIa in Fig. 12A). The Jaaninoja zone and parallel subsidiary zones form a prominent structural domain in the eastern part of the study area. As the NE-SW-trending zones show at least partial termination against the NNE–SSW-trending zones, the latter are older in their relative age. Zone III aligns with the previous interpretations (Väisänen and Hölttä 1999) as it intersects the Group I zone. Moreover, new, shorter parallel zones on the mainland have now been identified. The newly identified, shorter, and relatively evenly spaced structures with varying trends are clustered into Groups IV and V, with individual structures (VIa and VIb in Fig. 12A) located in the southern and northern parts of the area. Group IV follows the same orientation as a previously interpreted shear zone, mostly located offshore (IV and III in Fig. 12A). Due to limited data in the offshore area, no major depressions were observed there, but it is possible that a longer deformation zone exists offshore, representing this structural trend. Overall, the observed structures create a complex bedrock topography dominated by the intersecting and terminating features of Groups I, II, and III, where groups I and III form continuous and straight structures, while Group II is more discontinuous and contains segmented step-over structures.

The E-W trending deformation zones (Fig. 12A, Group I and V) are subparallel to the regional foliation (Fig. 12B) and, hence in line with an earlier interpretation attributing them to shearing along fold limbs during late stage folding (Väisänen and Hölttä 1999). The N-S trending deformation zones (Fig. 12A, Group III and IV) crosscut the foliation (Fig. 12B) and according to Väisänen and Hölttä (1999) are formed during the subsequent regional uplift. The orientations of the new deformation zones identified in this study partly follow the foliation: group II trends are parallel to the foliation in those areas where foliation data are available, whereas the southernmost tip of the deformation zones appear to crosscut the regional foliation. The tectonic phase

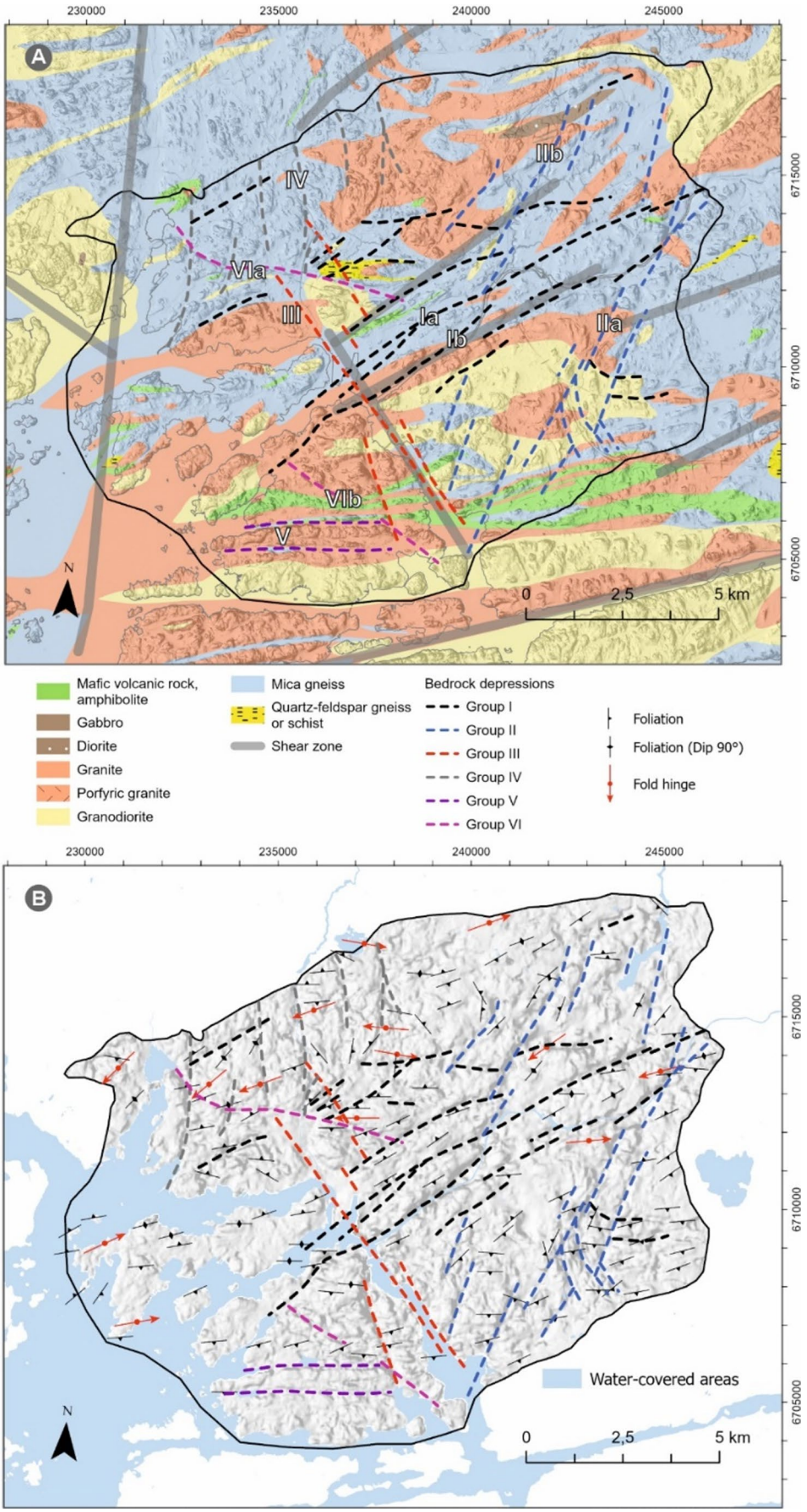

Fig. 12 (**A**) Bedrock lithology and shear zones modified after Lindberg et al. (1994), Väisänen and Hölttä (1999), and Väisänen (2007) and linear topographic depressions interpreted from the bedrock-DEM. Multidirectional hillshading was generated using LiDAR data (Laser scanning data 0.5 p, 2008–2019 @ NLS). (**B**) Linear topographic depressions, foliation and fold axial plunges modified after Lindberg et al. (1994) and Väisänen (2007). Multidirectional hillshading as background image, was generated using digital elevation model (Elevation model 2 m @ NLS)

to which these structures belong remains unresolved in this study.

In Turku area, the spatial occurrence and thickness of clayey deposits (Unit 3) and the underlying coarse-grained deposits (Unit 2) is largely controlled by both fine- and broad-scale topographic variability of the bedrock surface that in turn is shaped by the interplay of brittle bedrock structures and subsequent glacial erosion. The thickness of coarse-grained deposits vary greatly, forming thick layers in parts of valleys, while on slopes, such deposits may be entirely absent. The Laitilanharju ridge (I in Fig. 11) represents a distinct glaciofluvial unit within the area, differing from the rest of the region in terms of coarse-grained deposition. As expected for wide, low-energy basins, clay deposition initiated in the lowest parts of the bedrock topography and accumulated in valley- and basin-like depressions. This agreement with established sedimentological patterns supports the geological interpretation and validates that the model reproduces realistic sediment distribution across successive deep and shallow water phases of the BSB history.

The thickest fine-grained sediment deposits are formed in the deepest parts of these basins and depressions, which also have maintained continuous and relative high rate of sediment deposition since pro-glacial sedimentary environment (Ojala et al. 2021; Saresma et al. 2021). The development of the Aurajoki Valley in the central part of the area, during various phases of the Baltic Sea, marks a significant phase in the geological history of the Turku region. The valley originally formed in a deep bedrock depression shaped by a SW–SE-oriented deformation zone and broader depressions to the northeast of the main basin (II in Fig. 10). Over time, it was gradually filled with sediments as the land uplifted. Today, the Aurajoki Valley is one of the most prominent and thickest clayey basins in the Turku region. The Jaaninoja zone has had a sedimentary environment similar to the Aurajoki Valley, but it has been more isolated and is not associated with depressions as large and extensive. Both valleys consist, in the BTM paleotopographic model, of a central basin area surrounded by a wide depression particularly in the northern part of the valley. A third similar valley-like feature (I in Fig. 10) is partly located offshore, and due to the lack of data, its extent could not be assessed in this study.

In addition to improving structural interpretation, the 3D model highlights areas where subsurface information is sparse and interpolation uncertainty is elevated. These data gaps indicate locations where an additional borehole or targeted geophysical survey could substantially reduce uncertainty and enhance the accuracy of the model. Importantly, new geotechnical investigations are continuously conducted in the Turku area, and as this new information becomes available, the model can be iteratively updated and progressively refined. This continuous improvement makes the model a dynamic tool that evolves alongside expanding subsurface datasets. Furthermore, the model enables several types of derivative outputs that support practical applications, including predicted ground conditions at specific locations, longitudinal profiles along planned infrastructure corridors, cross sections illustrating variations in bedrock elevation and sediment thickness, and thematic maps representing different ground conditions such as soft soil distribution or bedrock depth. In addition, the modelled surfaces allow a simplified delineation of domains based on the presence and thickness of superficial units, such as areas dominated by clay, areas containing coarse-grained deposits, and areas where thin or thick coarse-grained layers underlie clay. Together, these outputs translate the regional scale 3D model into actionable information for engineering design, feasibility assessment, and early-stage urban and infrastructure planning.

Conclusions

This study demonstrates the feasibility and value of integrating topographic data, geological mapping, and various types of geotechnical investigation to develop geologically realistic 3D models of subsurface conditions in urban environments. In the Turku area, the models reveal substantial topographic variation, including steep bedrock slopes, sharp features, and thick accumulations of glacial and postglacial sediments—features that pose challenges for construction and underground planning. The occurrence of these deposits is primarily controlled by bedrock topography, with depressions acting as sediment accumulation environments, highlighting the need for an integrated modelling approach that considers both bedrock and overburden components.

A simplified classification and careful selection of geological units (Units 1–3) enables efficient and informative visualization of complex geology and its geotechnical properties at the regional scale, offering a practical tool for city-scale land use planning and major construction projects. However, for site-specific applications, the 3D analysis must be expanded, as demonstrated by Ojala et al. (2021) in the Rastaala area in Espoo, southern Finland. In practice, proposed engineering works would still require further site investigations to characterise local geotechnical conditions, but the planning and subsequent implementation of such works are substantially assisted by the regional-scale information provided by the present modelling.

Future improvements could include automation of bedrock surface modelling using artificial intelligence for outcrop delineation and scripting for data processing and error correction. A reliability map would support structural

interpretation and provide clearer visualization of model uncertainty, which naturally varies across the model depending on the spacing of available data points and the heterogeneity of the geological conditions. Overall, the resulting 3D models represent a significant advancement from traditional 2D approaches, combining geological evolution, sediment deposition, and extensive datasets into a coherent framework. While based on simplified geological structures, these models already provide a valuable generalization for urban planning, construction, and zoning, provided that the conceptual model is carefully designed to reflect the complexity of regional geology and the available data.

Acknowledgements We gratefully acknowledge Novatron for providing an academic license for the 3D-Win software, which was essential for processing geotechnical investigation data. We also thank the City of Turku for granting access to their geotechnical datasets. We would like to thank Laura Pirilä for sharing data from her previous work, which supported this study. We further acknowledge Emilia Kosonen and Noora Hornborg from the Geological Survey of Finland (GTK) for their valuable assistance in processing geotechnical data for clay modelling. We also gratefully acknowledge the Finnish Cultural Foundation – Southwest Finland Regional Fund for funding the MSc theses that provided an important foundation for this work.

Author contributions KA conceptualized the study and wrote the original draft. KA, PS, NA, AO and ER collected and analysed the data, prepared figures, interpreted the results and reviewed the manuscript.

Funding Open Access funding provided by Geological Survey of Finland.

Declarations

Conflict of interest The authors declare no competing interests.

References

Ahlqvist K (2023) Turun alueen erodoituneen kallioperän yläpinnan 3D-mallinnus geoteknisten kairausten avulla. MSc thesis, University of Turku, Finland. Available at: https://urn.fi/URN:NBN:fi-fe2023072691538

Anttila N (2023) Construction of 3D clay thickness models of Turku for urban planning and infrastructure. MSc thesis, University of Turku, Finland. Available at: https://urn.fi/URN:NBN:fi-fe2023050942263

Artimo A, Mäkinen J, Berg RC, Abert CC, Salonen V-P (2003) Three-dimensional geologic modeling and visualization of the Virttaankangas aquifer, southwestern Finland. Hydrogeol J 11:378–386. https://doi.org/10.1007/s10040-003-0256-6

Björck S (1995) A review of the history of the Baltic Sea, 13.0–8.0 ka BP. Quatern Int 27:19–40. https://doi.org/10.1016/1040-6182(94)00057-C

Bouchard MA, Gibbard P, Salonen V-P (1990) Lithostratotypes for Weichselian and pre-Weichselian sediments in southern and western Finland. Bull Geol Soc Finland 62:79–95. https://doi.org/10.17741/bgsf/62.1.005

Boulton GS (1978) Boulder shapes and grain-size distributions of debris as indicators of transport paths through a glacier and till genesis. Sedimentology 25:773–799. https://doi.org/10.1111/j.1365-3091.1978.tb00329.x

Boulton G, Dongelmans P, Punkari M, Broadgate M (2001) Palaeoglaciology of an ice sheet through a glacial cycle: the European ice sheet through the Weichselian. Q Sci Rev 20:591–625. https://doi.org/10.1016/S0277-3791(00)00160-8

Collon P, Steckiewicz-Laurent W, Pellerin J, Laurent G, Caumon G, Reichart G, Vaute L (2015) 3D geomodelling combining implicit surfaces and Voronoi-based remeshing: A case study in the Lorraine Coal Basin (France). Comput Geosci 77:29–43. https://doi.org/10.1016/j.cageo.2015.01.009

Culshaw MG (2005) From concept towards reality: developing the attributed 3D geological model of the shallow subsurface. QJEGH 38:231–284. https://doi.org/10.1144/1470-9236/04-072

Devleeschouwer X, Pouriel F (2009) Brussels Urban Geology (BUG): a 2D and 3D model of the underground by means of GIS. In M. G. Culshaw, H. J. Reeves, I. Jefferson & T. W. Spink (Eds.) Engineering Geology for Tomorrow's Cities (Engineering Geology Special Publication No. 22, Paper 420, 1–9

Donner J (1995) The quaternary history of Scandinavia, l. paperback version. ed, World and regional geology. Cambridge University Press, Cambridge

Edén P, Boman A, Mattbäck S, Auri J, Yli-Halla M, Österholm P (2023) Mapping, impacts, characterization and extent of acid sulfate soils in Finland. Bull Geol Soc Finland 95:135–160. https://doi.org/10.17741/bgsf/95.2.003

El May M, Dlala M, Chenini I (2010) Urban geological mapping: Geotechnical data analysis for rational development planning. Eng Geol 116:129–138. https://doi.org/10.1016/j.enggeo.2010.08.002

Finnish Environmental Institute (2021) Shoreline 10 and river network [Geospatial dataset]. Available at: https://ckan.ymparisto.fi/dataset/ranta10-rantaviiva-1-10-000 [Accessed 28.12.2022]

Fookes P.G. (1997) Geology for Engineers: the Geological Model, Prediction and Performance. QJEGH 30:293–424. https://doi.org/10.1144/GSL.QJEG.1997.030.P4.02

Gardemeister R (1973) Hienorakeisten maalajien geologisia ja geoteknisiä tutkimustuloksia, Tiedonanto / Geotekniikan Laboratorio, Valtion Teknillinen Tutkimuskeskus. Valtion Teknillinen Tutkimuskeskus, Otaniemi

Geological Survey of Finland (2022) Bedrock of Finland 1:200 000. Version 2.3. [ArcGIS filegeodatabase] Available at: https://hakku.gtk.fi/en/locations/search?location_id=181 [Accessed: 1.3.2025]

Geological Survey of Finland (2015) Superficial Deposits 1:20 000/1:50 000. Version 1.0. [ArcGIS filegeodatabase] Available at: https://hakku.gtk.fi/en/locations/search?location_id=181 [Accessed: 1.3.2025]

Glückert G (1976) Post-glacial shore-level displacement of the Baltic in SW Finland Annales Academiae Scientiarum Fennicae. Series A. 3, Geologica, geographica. Suomalainen Tiedeakatemia, Helsinki

Heinonen S, Snyder D, Heikkinen P, Kukkonen I (2012) Use of seismic reflection profiling for 3D-modeling of mineralized regions: A case study from Pyhäsalmi, Finland. Presented at the The 43rd Nordic Seismology Seminar, Tallinn, Estonia, p. 11

Hirvas H, Nenonen K (1987) The till stratigraphy of Finland, in: INQUA Till Symposium, Finland 1985, Special Paper. Geological Survey of Finland, Espoo, p. 194

Hirvas H, Lintinen P, Lunkka JP, Eriksson B, Grönlund T (1995) Sedimentation and lithostratigraphy of the Vuosaari multiple till sequence in Helsinki, southern Finland. Bull Geol Soc Finland 67:51–64. https://doi.org/10.17741/bgsf/67.2.004

Kaskela AM, Kotilainen AT, Al-Hamdani Z, Leth JO, Reker J (2012) Seabed geomorphic features in a glaciated shelf of the Baltic Sea. Estuar Coast Shelf Sci 100:150–161. https://doi.org/10.1016/j.ecss.2012.01.008

Knill J (2003) Core values: the first Hans-Cloos lecture. Bull Eng Geol Environ 62:1–34. https://doi.org/10.1007/s10064-002-0187-9

Koistinen T, Stephens MB, Bogatchev V, Nordgulen Ø, Wennerström M, Korhonen J (2001) Geological map of the Fennoscandian shield. Geological Surveys of Finland, Norway and Sweden and Ministry of Natural Resources of Russia Federation

Krabbendam M, Bradwell T (2014) Quaternary evolution of glaciated gneiss terrains: pre-glacial weathering vs. glacial erosion. Q Sci Rev 95:20–42. https://doi.org/10.1016/j.quascirev.2014.03.013

Lahtinen R, Korja A, Nironen M (2005) Chapter 11 Paleoproterozoic tectonic evolution. Developments in Precambrian Geology. Elsevier, pp 481–531. https://doi.org/10.1016/S0166-2635(05)80012-X

Lindberg B, Ehlers C, Edén P (1994) Suomen geologinen kartta: kallioperäkartta. Lehti 1043, Turku. Geologian tutkimuskeskus, Espoo

Lindqvist T, Ruuska E, Kosonen E, Hornborg N, Skyttä P, Putkinen N, Mansikkamäki J (2025) Integrated geological modeling of partially exposed Precambrian bedrock surface and thickness of overlying Quaternary deposits. Eng Geol 346:107902. https://doi.org/10.1016/j.enggeo.2024.107902

Lounais-Suomen Seutukaavaliitto (1966) Turun seudun geologisen maaperäkartoituksen selitys vuodelta 1966. Turku

Lundblad ER, Wright DJ, Miller J, Larkin EM, Rinehart R, Naar DF, Donahue BT, Anderson SM, Battista T (2006) A Benthic Terrain Classification Scheme for American Samoa. Mar Geodesy 29:89–111. https://doi.org/10.1080/01490410600738021

Malinowski M, Putkinen N, Brodic B, Laakso V, Koskela E, Heinonen S, Engström J, Paananen M (2023) P- and S-wave Seismic Imaging of a Complex Aquifer System in Kurikka, Western Finland. First Break 41:67–72. https://doi.org/10.3997/1365-2397.fb2023063

National Land Survey of Finland (2024a) Elevation model 10 m.[GEOTiff] Available at: https://avoin-paikkatieto.maanmittauslaitos.fi/tiedostopalvelu/ogcproc/v1/ [Accessed at 1.3.2025]

National Land Survey of Finland (2024b) Elevation model 2 m. [GEOTiff] Available at: https://avoin-paikkatieto.maanmittauslaitos.fi/tiedostopalvelu/ogcproc/v1/ [Accessed at 1.3.2025]

Niemelä J, Stén C-G, Taka M, Winterhalter B (1987) Turun-Salon seudun maaperä: Maaperäkarttojen selitykset, explanation to the maps of quaternary deposits, Suomen geologinen Kartta 1:100 000. Geologian Tutkimuskeskus, Espoo

Ojala AEK (2011) Construction suitability and 3D architecture of fine-grained sedimentary deposits in southern Finland – examples from Espoo. In: Nenonen K, Nurmi PA (eds) Geoscience for Society 125th Anniversary Volume, Special Paper. Geological Survey of Finland, Espoo, p 357

Ojala AEK, Palmu J-P, Åberg A, Åberg S, Virkki H (2013) Development of an ancient shoreline database to reconstruct the Litorina Sea maximum extension and the highest shoreline of the Baltic Sea basin in Finland. Bull Geol Soc Finland 85:127–144. https://doi.org/10.17741/bgsf/85.2.002

Ojala AEK, Saresma M, Virtasalo JJ, Huotari-Halkosaari T (2018) An allostratigraphic approach to subdivide fine-grained sediments for urban planning. Bull Eng Geol Environ 77:879–892. https://doi.org/10.1007/s10064-016-0981-4

Ojala AEK, Virtasalo JJ, Lindsberg E, Markovaara-Koivisto M (2021) Basin-Scale 3D Sedimentary Modelling: An Approach to Subdivide Baltic Sea Onshore Sediments for Land use and Construction. Geotech Geol Eng 39:4855–4876. https://doi.org/10.1007/s10706-021-01799-8

Palacios D, Hughes PD, García-Ruiz JM, Andrés N (2022) The Quaternary ice ages, in: European Glacial Landscapes: Maximum Extent of Glaciations. Elsevier, Oxford, p 522

Patton H, Hubbard A, Heyman J, Alexandropoulou N, Lasabuda APE, Stroeven AP, Hall AM, Winsborrow M, Sugden DE, Kleman J, Andreassen K (2022) The extreme yet transient nature of glacial erosion. Nat Commun 13:7377. https://doi.org/10.1038/s41467-022-35072-0

Pirilä L (2016) Savikerrostumien syntyhistoria, niiden paksuus- ja ominaisuusvaihtelut sekä vaikutukset yhdyskuntatekniikkaan Turun alueella (Pro gradu -tutkielma). Turun yliopisto

Rainio H, Lahermo P (1976) Observations on dark grey basal till in Finland. Bull Geol Soc Finland 48:137–152. https://doi.org/10.17741/bgsf/48.1-2.011

Rinne H, Kaskela A, Downie A-L, Tolvanen H, Von Numers M, Mattila J (2014) Predicting the occurrence of rocky reefs in a heterogeneous archipelago area with limited data. Estuar Coast Shelf Sci 138:90–100. https://doi.org/10.1016/j.ecss.2013.12.025

Ruuska E, Skyttä P, Putkinen N, Valjus T (2023) Contribution of bedrock structures to the bedrock surface topography and groundwater flow systems within deep glaciofluvial aquifers in Kurikka, Western Finland. Earth Surf Processes Landf 48:2039–2056. https://doi.org/10.1002/esp.5602

Saresma M, Kosonen E, Ojala AEK, Kaskela A, Korkiala-Tanttu L (2021) Characterization of sedimentary depositional environments for land use and urban planning in Espoo, Finland. Bull Geol Soc Finland 93:31–51. https://doi.org/10.17741/bgsf/93.1.003

Saresma M, Löfman M, Kosonen E, Ojala AEK, Korkiala-Tanttu L (2023) Statistical approach to identify variables predicting sulphide clay occurrence in southern Finland. Bull Eng Geol Environ 82:257. https://doi.org/10.1007/s10064-023-03258-5

Skyttä P, Mänttäri I (2008) Structural setting of late Svecofennian granites and pegmatites in Uusimaa Belt, SW Finland: Age constraints and implications for crustal evolution. Precambrian Res 164:86–109. https://doi.org/10.1016/j.precamres.2008.04.001

Skyttä P, Kinnunen J, Palmu J-P, Korkka-Niemi K (2015) Bedrock structures controlling the spatial occurrence and geometry of 1.8Ga younger glacifluvial deposits — Example from First Salpausselkä, southern Finland. Glob Planet Change 135:66–82. https://doi.org/10.1016/j.gloplacha.2015.10.007

Skyttä P, Nordbäck N, Ojala A, Putkinen N, Aaltonen I, Engström J, Mattila J, Ovaskainen N (2023) The interplay of bedrock fractures and glacial erosion in defining the present-day land surface topography in mesoscopically isotropic crystalline rocks. Earth Surf Processes Landf 48:1956–1968. https://doi.org/10.1002/esp.5596

Stroeven AP, Hättestrand C, Kleman J, Heyman J, Fabel D, Fredin O, Goodfellow BW, Harbor JM, Jansen JD, Olsen L, Caffee MW, Fink D, Lundqvist J, Rosqvist GC, Strömberg B, Jansson KN (2016) Deglaciation of Fennoscandia. Q Sci Rev 147:91–121. https://doi.org/10.1016/j.quascirev.2015.09.016

Väisänen M (2007) Suomen geologinen kartta: kallioperäkartta. Lehti 1044. Geologian tutkimuskeskus, Espoo

Väisänen M, Hölttä P (1999) Structural and Metamorphic Evolution of the Turku Migmatite Complex, Southwestern Finland. Bull Geol Soc Finl 71:177–218

Virtasalo JJ, Hämäläinen J, Kotilainen AT (2014) Toward a standard stratigraphical classification practice for the B altic S ea sediments: the CUAL approach. Boreas 43:924–938. https://doi.org/10.1111/bor.12076

Walbridge S, Slocum N, Pobuda M, Wright D (2018) Unified Geomorphological Analysis Workflows with Benthic Terrain Modeler. Geosciences 8:94. https://doi.org/10.3390/geosciences8030094

Wang Z, Qu H, Wu Z, Wang X (2018) Geo3DML: A standard-based exchange format for 3D geological models. Comput Geosci 110:54–64. https://doi.org/10.1016/j.cageo.2017.09.008